# Influence of 3d transition-metal substitution on the oxygen reduction reaction electrocatalysis of ternary nitrides in acid

Kevin E. Fritz<sup>1</sup>, Yichen Yan<sup>1</sup>, and Jin Suntivich<sup>1,2</sup> (\subseteq)

- <sup>1</sup> Department of Materials Science and Engineering, Cornell University, Ithaca, New York 14850, USA
- <sup>2</sup> Kavli Institute at Cornell for Nanoscale Science, Ithaca, New York 14850, USA

© Tsinghua University Press and Springer-Verlag GmbH Germany, part of Springer Nature 2019 **Received:** 19 February 2019 / **Revised:** 7 May 2019 / **Accepted:** 16 May 2019

### **ABSTRACT**

The development of non-precious, acid-stable, oxygen reduction reaction (ORR) electrocatalysts can significantly aid the commercialization of proton exchange membrane fuel cells (PEMFCs). We report a survey of the ORR electrocatalysis on 3d metal substituted (M = Mn, Fe, Co) molybdenum and tungsten nitrides in acidic environments. We find that molybdate catalysts are more active than tungstates, with the specific activity depending on the chemistry of the substituted 3d metal. In both families, more electronegative 3d metals led to higher ORR activity (i.e., Co > Fe > Mn). We attribute this result to the ability of the more electronegative 3d metal to withdraw electrons from the Mo- or W-based active sites, effectively oxidizing the metal centers of the catalysts. Based on our observation, future nitride ORR electrocatalysts can be further optimized by oxidizing the Mo sites further by, for example, adding even more electronegative dopant metals or incorporating anion vacancies.

### **KEYWORDS**

nitrides, electrocatalysis, fuel cells, oxygen reduction

The oxygen reduction reaction (ORR:  $O_2 + 4H^+ + 4e^- \rightarrow 2H_2O$ ) represents the largest source of inefficiency in proton exchange membrane fuel cells (PEMFCs) [1]. While Pt-based electrocatalysts have shown promising activity for the ORR in acid [2, 3] mimicking the PEMFC environment [4], their limited abundance restricts the long-term scalability of PEMFCs. So far, graphitic carbon nanostructures containing nitrogen-complexed 3d transition metals (M-N-C) are the only alternative for the ORR in acid [5-8]; however, several issues have hindered their widespread adoption, for example, poor stability and low active site density/utilization [9]. These limitations motivate us to examine transition metal nitrides (TMNs) as alternative acid-stable ORR catalysts. Considering that TMNs consist entirely of M-N moieties, the high active site densities may eventually allow TMNs to be even more active than M-N-C catalysts. In addition, their crystallinity may provide greater stability and corrosion resistance which are currently restrictions of M-N-C catalysts.

In this work, we survey how the addition of late transition metals (Mn, Fe, and Co) to early transition metal nitrides (Mo and W) can influence the ORR kinetics. Co, Fe, and Mn nitrides and oxynitrides are active in alkaline [10–13]; however, they are not stable under acidic conditions [14]. Early transition metals such as group 4–5 nitrides are stable at low pH but show modest ORR activity [15]. The best of both worlds is obtained when the early and late TMNs are combined, e.g., Fe<sub>0.8</sub>Mo<sub>1.2</sub>N<sub>2</sub> and Co<sub>0.6</sub>Mo<sub>1.4</sub>N<sub>2</sub>, which are active and stable for the ORR in acid [16, 17]. Similarly, FeWN<sub>2</sub> has been reported to be stable at low pH [18]. While the activity of these TMN compounds is known to depend on their composition, the underlying reason for the performance variation is unclear. Several studies seeking to understand the electrocatalytic activity trend

have had challenges, including characterization difficulties with the nature of the catalysts or that the model catalysts do not have sufficient stability to establish robust structure–property relations. A prominent example is VN, where late 3d metal substitution can enhance the ORR activity [19], which has been attributed to changing the V valence. However, the activity of the substituted VN degrades in < 10 cycles, making it difficult to analyze the structure–property relationship.

To help understand the structure-property relations of TMNs, we study a series of stable, isostructural TMNs, where the composition can be varied without significantly altering the local structure and coordination [17, 19]. This selection allows us to focus on the influence of 3d transition metal addition. The model catalysts are Mn, Fe, and Co nitrides substituted into W and Mo nitrides. Each of these compounds crystallizes in an ordered, layered hexagonal structure with formula  $MXN_2$  (M = Mn, Fe, Co; X = Mo, W), which has been shown to be stable in acid. Apart from MnWN<sub>2</sub>, whose coordination environment is still a subject of debate [20, 21], all studied structures consist of alternating octahedral and trigonal prismatic coordination environments, where the 3d metals prefer the layers with octahedral coordination while Mo or W prefer ones with trigonal prismatic ordering (Fig. 1). Because all the studied samples are ordered and isostructural, their comparison allows a systematic survey of the effect of the 3d metal substitution in the TMNs without any interference from structure variations and/or heterogeneity in the cation distribution.

We characterize the ORR activity of ternary vs. binary nitrides using Mo- and W-containing nitrides as baseline binary compounds. Molybdenum nitride with a Mo<sub>2</sub>N crystal structure was synthesized by heating ammonium heptamolybdate under flowing NH<sub>3</sub> at 700 °C



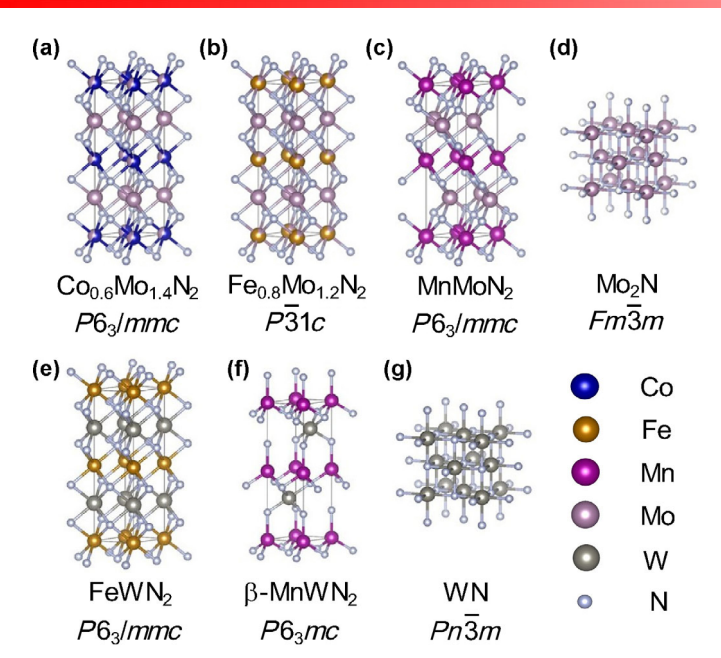


Figure 1 Structure and space group of binary and ternary nitrides studied in this work: (a)  $Co_{0.6}Mo_{1.4}N_2$ , (b)  $Fe_{0.8}Mo_{1.2}N_2$ , (c)  $MnMoN_2$ , (d)  $Mo_2N$ , (e)  $FeWN_2$ , (f) β-MnWN<sub>2</sub> and (g) WN.

for 3 h, while tungsten nitride (WN) was synthesized by heating ammonium metatungstate under flowing NH3 at 700 °C for 5 h. For ternary nitrides, the samples were synthesized by first preparing ternary oxides at the desired stoichiometries, then nitriding the ternary oxides into ternary nitrides. To prepare the ternary oxides in the first step, we followed procedures adapted from Refs. [17, 20, 22-24]. Starting with the Mo-containing TMNs, MnMoO4 and CoMoO<sub>4</sub> were prepared as precursors by mixing ammonium heptamolybdate with manganese(II) nitrate or cobalt(II) nitrate in deionized water with a 1:1 molar ratio of metal atoms and heating at 120 °C overnight. The resulting powder was then heated at 700 °C for 12 h under room air to crystallize the ternary oxide. Iron molybdenum oxide was formed similarly by first preparing 15 mL of 0.67 M Na<sub>2</sub>MoO<sub>4</sub> and 40 mL of 0.25 M FeCl<sub>2</sub>. The aqueous solutions were then mixed by adding FeCl2 dropwise to the molybdenum solution under vigorous stirring. A dark brown solid precipitated and the solution was stirred for 1 h to allow the reaction to go to completion. The resulting precipitate was collected, vacuum dried, and washed twice with deionized water and once with ethanol before drying overnight at 120 °C.

After obtaining the precursor oxides, the materials were heated under flowing  $NH_3$  to form ternary nitrides. The Co/Mo- and Fe/Mo-containing nitrides were formed using a two-step process. The first step involves heat treatment of the ternary oxides for 12 h under  $NH_3$  at high temperature to form  $Co_3Mo_3N$  (700 °C) and  $Fe_3Mo_3N$  (800 °C) subnitrides. In the second heating step, the final ternary TMNs were formed by heating for 6 h at 400 °C. We used a one-step process for MnMoN<sub>2</sub>, which was formed directly by heating the ternary oxide at 625 °C for 24 h under  $NH_3$ .

Ternary W oxides used as precursors for the syntheses of W-based TMNs were synthesized using a similar co-precipitation method. Specifically, 40 mL of 0.25 M FeCl<sub>2</sub> or 0.25 M Mn(NO<sub>3</sub>)<sub>2</sub> was added dropwise to 15 mL of 0.67 M Na<sub>2</sub>WO<sub>4</sub>, stirred for 1 h, and then washed twice with deionized water and once with ethanol before drying overnight at 120 °C. The final nitrides were then formed by a one-step heating of the corresponding oxides at 700 °C for 12 h (FeWN<sub>2</sub>) or 800 °C for 24 h (MnWN<sub>2</sub>) under flowing NH<sub>3</sub>.

We characterize the crystal structures of both the precursors and final compounds using X-ray diffraction (XRD). We first examine the oxide precursors. For Mo-containing oxides, both MnMoO<sub>4</sub>

and CoMoO<sub>4</sub> had a monoclinic structure with space group C12/m1 (No. 12) (Figs. S1 and S2 in the Electronic Supplementary Material (ESM)), while FeMoO<sub>x</sub> had an amorphous structure. For W-containing oxides, both MnWO<sub>x</sub> and FeWO<sub>x</sub> had amorphous structures after drying at 120 °C. To prepare the ternary TMN compounds, we first used heat treatment to convert CoMoO<sub>4</sub> and FeMoO<sub>x</sub> to Co<sub>3</sub>Mo<sub>3</sub>N and Fe<sub>3</sub>Mo<sub>3</sub>N subnitrides (Figs. S3 and S4 in the ESM) [25]. These sub-nitrides, which were formed in the first part of the two-step heat treatment, crystallize in the cubic space group  $Fd\overline{3}m$  and consist of 3d metals residing between Mo<sub>6</sub>N moieties. After forming these initial subnitrides, the next heat-treatment step was used to incorporate more nitrogen, effectively transforming the subnitrides into nitrides. To do this, we annealed Co<sub>3</sub>Mo<sub>3</sub>N and Fe<sub>3</sub>Mo<sub>3</sub>N at lower temperature under NH<sub>3</sub>. During this second nitridation step, the structures rearrange to a layered hexagonal structure.

At this point, we must point out that the final metal stoichiometries of the TMNs are difficult to control. This is in part due to the complex nitrogen-incorporation kinetics and the propensity of the TMNs to reject 3d metals from the lattice as an impurity phase. Using high temperature to increase the mixing entropy faces the challenge that the nitrogen atoms may leave in the gas-phase or that ternary structures will phase-separate while lower temperatures may limit the atomic diffusion needed for anion exchange. The syntheses reported herein were developed through empirical optimization building on literature results. In each nitride synthesis, the target structure was cooled quickly by opening the top of the flow furnace and removing the furnace tube from the hot zone, reaching temperatures < 100 °C in ~ 15 min. Allowing the furnace to cool slowly under ambient conditions resulted in phase-separation of the final product. Additionally, controlling the NH<sub>3</sub> flow rate was critical for achieving phase-pure results. For subnitrides, Co<sub>3</sub>Mo<sub>3</sub>N and Fe<sub>3</sub>Mo<sub>3</sub>N, a low flow rate (50 mL·min<sup>-1</sup>) was required, while faster flow rates produced a mixture of the layered hexagonal phase with several impurity phases such as molybdenum nitrides, cobalt, and iron nitride. Similarly, for the layered hexagonal phases, a higher flow rate (150 mL·min<sup>-1</sup>) was required for complete conversion to the N-rich phase from both oxide and subnitride precursors. In the case of Co<sub>0.6</sub>Mo<sub>1.4</sub>N<sub>2</sub> and Fe<sub>0.8</sub>Mo<sub>1.2</sub>N<sub>2</sub>, however, the highly reducing NH<sub>3</sub> environment precluded formation of a phase-pure TMN at all flow rates and cooling rates studied, consistent with previous reports [17]. So, to avoid the possibility that the impurity phases may affect characterization of the final stoichiometries, these impurity phases were removed using acid treatment. The final stoichiometries were analyzed post-synthesis using energy-dispersive X-ray spectroscopy (EDS, vide infra). We find that the EDS compositions are in good agreement with literature and have chosen to label the formula with previously reported stoichiometries to facilitate a comparison to literature.

The XRD spectra of the final TMN compounds (Figs. 2(a) and 2(b)) are consistent with the TMN structures presented in Fig. 1. Mo<sub>2</sub>N (a = 4.18 Å) has a rock salt structure with the space group  $Fm\overline{3}m$ (No. 225). In this structure, the stoichiometric compound has vacancies in the anionic sites as Mo is not fully oxidized under the reducing condition of NH<sub>3</sub>; however, based on thermogravimetric analysis (TGA), a significant fraction of the anion sites were found to be filled with residual oxygen (Fig. S5(a) in the ESM). WN (a =4.14 Å) crystallizes in the closely related  $Pn\overline{3}m$  (No. 224) space group; however, we again note the presence of residual oxygen from TGA (Fig. S5(b) in the ESM). For  $Co_{0.6}Mo_{1.4}N_2$  (a = 2.86 Å; c =10.98 Å), MnMoN<sub>2</sub> (a = 2.92 Å; c = 10.86 Å), and FeWN<sub>2</sub> (a = 2.87 Å; c = 10.97 Å) the XRD spectra are consistent with a layered hexagonal structure with the space group P63/mmc (No. 194), while the XRD pattern for Fe<sub>0.8</sub>Mo<sub>1.2</sub>N<sub>2</sub> (a = 2.85 Å; c = 11.01 Å) is consistent with the closely related  $P\overline{3}1c$  space group (No. 163). For the case of MnMoN<sub>2</sub>, the PDF entry (PDF 01-086-0786) lists a stacking sequence

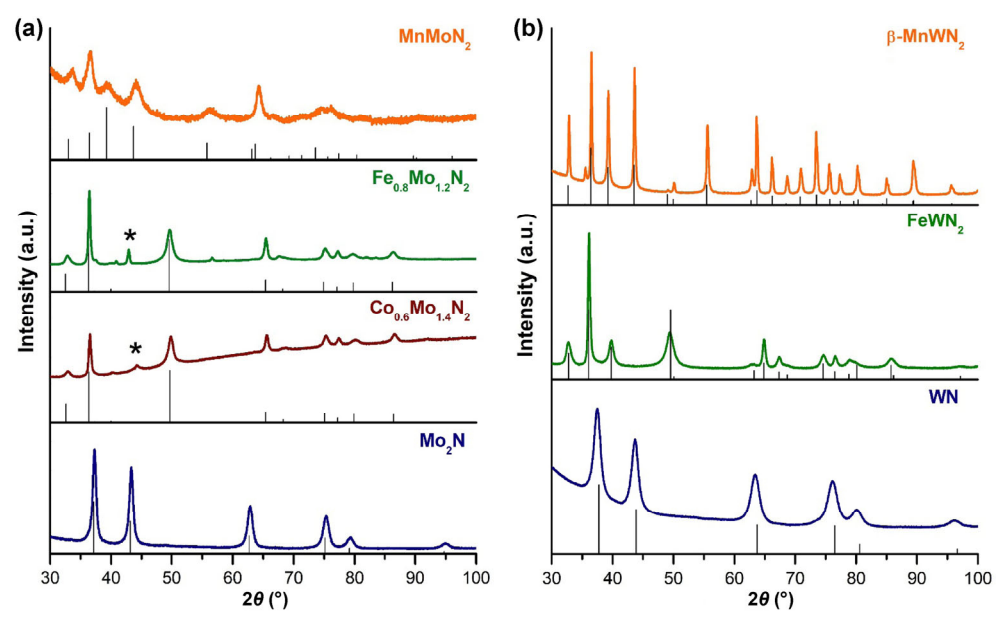


Figure 2 (a) XRD pattern for molybdenum-containing nitrides. MnMoN<sub>2</sub> matches with PDF 01-086-0786, Fe<sub>0.8</sub>Mo<sub>1.2</sub>N<sub>2</sub> with PDF 01-086-0197, and Mo<sub>2</sub>N with PDF 01-025-1366. Co<sub>0.6</sub>Mo<sub>1.4</sub>N<sub>2</sub> does not have a PDF entry, however, our result is consistent with previous reports. The impurity phase in Co<sub>0.6</sub>Mo<sub>1.4</sub>N<sub>2</sub> is metallic Co (PDF 01-089-4307), and the impurity phase in Fe<sub>0.8</sub>Mo<sub>1.2</sub>N<sub>2</sub> is Fe<sub>2</sub>N (PDF 01-073-2102). (b) XRD pattern for tungsten-containing nitrides. β-MnWN<sub>2</sub> matches with PDF 01-083-0924, FeWN<sub>2</sub> with PDF 01-086-0785, and WN with PDF 01-075-1012.

that is unphysical; we have therefore used a structure with a more appropriate stacking sequence that has been reported in Ref. [23]. There is no PDF entry for Co<sub>0.6</sub>Mo<sub>1.4</sub>N<sub>2</sub>, however, our result is consistent with the neutron and synchrotron X-ray scattering results reported by Khalifah and colleagues [17, 26]. Each of these structures consists of alternating layers of edge-shared octahedra and trigonal prisms. The trigonal prismatic environments are occupied by Mo or W, while the octahedral environments are predominantly occupied by the 3d transition metals. In the case of Fe<sub>0.8</sub>Mo<sub>1.2</sub>N<sub>2</sub> and Co<sub>0.6</sub>Mo<sub>1.4</sub>N<sub>2</sub>, prior studies in literature have suggested that some Mo may fill in the octahedral sites [22, 26], which are created as the material rejects the 3d transition metals during nitridation. These rejected 3d metals phase-separate into an impurity phase (15.4 wt.% for Co and 16.0 wt.% for Fe, the latter as a nitride). The stacking sequence for Fe<sub>0.8</sub>Mo<sub>1.2</sub>N<sub>2</sub>, Co<sub>0.6</sub>Mo<sub>1.4</sub>N<sub>2</sub>, and FeWN<sub>2</sub> is AcAcBcBcA, where A and B represent the close-packed N atoms and c represents the metal atoms. MnMoN2 has a slightly different stacking sequence due to the larger Mn ionic radii: AbAcBaBcA where A and B represent the close packed N atoms, c = manganese, and a, b = molybdenum. The coordination environment of each class of cations is the same in all compounds to allow for a systematic study. We show the extracted lattice parameters in Table S1 in the ESM.

We now discuss the structure of MnWN<sub>2</sub>, which has two polymorphs, each formed at different temperature that consist of different metal stacking sequences.  $\alpha$ -MnWN<sub>2</sub> has a stacking sequence of AABBCC, while  $\beta$ -MnWN<sub>2</sub> has ABACABAC. The XRD of MnWN<sub>2</sub> shows that our structure is  $\beta$ -MnWN<sub>2</sub> (a=2.93 Å; c=10.94 Å), which has been proposed to crystallize either in the  $P6_3/mmc$  (No. 194) or  $P6_3mc$  (No. 186) space group depending on the N lattice positions. Space group  $P6_3/mmc$  provides the best fit to the experimental data; however, we caution that the fitting represents an average structure because a simultaneous occupancy of adjacent N lattice positions would yield an unfeasible N–N bond distance. For a structure with a uniform N site occupancy,  $P6_3mc$ , which consists of alternating layers of MnN<sub>4</sub> tetrahedra and WN<sub>6</sub> octahedra coordination environments, would represent a more physically reasonable fit.

The exact metal stoichiometry of each nitride was determined using scanning electron microscopy (SEM) and EDS (Figs. S6-S10

and Table S2 in the ESM). The measured stoichiometries were 42:58, 53:47, and 58:42 for MnMoN<sub>2</sub>, MnWN<sub>2</sub>, and FeWN<sub>2</sub> (i.e., with the formula determined from EDS of Mn<sub>0.8</sub>Mo<sub>1.2</sub>N<sub>2</sub>, MnWN<sub>2</sub>, and Fe<sub>1.2</sub>W<sub>0.8</sub>N<sub>2</sub>). These results are close to literature reports of a 1:1 ratio when considering the intrinsic errors of the EDS measurement [20, 23]. Fe- and Co-containing molybdenum nitride were measured as-synthesized and acid-leached, using 0.1 M HClO<sub>4</sub> to remove the Co and Fe<sub>2</sub>N impurities. For the Fe/Mo-containing sample, the final stoichiometry was 0.7:1.3 Fe:Mo (i.e., Fe<sub>0.7</sub>Mo<sub>1.3</sub>N<sub>2</sub>) after acid leaching, in good agreement with the 2:3 metal ratio expected from Ref. [22]. After subtracting the 15.4 wt.% Co impurity observed in the XRD spectra, the as-synthesized Co/Mo-containing sample had a stoichiometry of Co<sub>0.9</sub>Mo<sub>1.1</sub>N<sub>2</sub>. Previous reports indicate similar EDS metal ratios but instead assign the stoichiometry Co<sub>0.6</sub>Mo<sub>1.4</sub>N<sub>2</sub> based on the refinement of synchrotron X-ray and neutron scattering data [17, 26]. A significant amount of cobalt was removed during acid leaching, however, resulting in a final stoichiometry of Co<sub>0.2</sub>Mo<sub>1.8</sub>N<sub>2</sub>. The morphology of each catalyst was also characterized using SEM (Fig. 3). The particles clustered together into aggregates with sizes varying between  $\sim$  12 to 45  $\mu$ m. We suspect that the observed morphology is a consequence of void creation and subsequent re-filling caused by the exchange of O and N anions during the syntheses.

The surface area and porosity of each sample were characterized using N2 adsorption. Brunauer-Emmett-Teller (BET) analysis showed that the specific surface area ranged from ~ 1 to 30 m<sup>2</sup>·g<sup>-1</sup>. As expected, samples were heated at higher temperatures and for longer durations showed lower specific surface area. Different isotherm types were observed for different samples. MnMoN2, Co0.6Mo1.4N2, and WN had typical type IV isotherms with H<sub>1</sub>-type hysteresis consistent with the presence of mesoporosity while other structures showed type II behavior, indicative of a nonporous morphology (Fig. S11 in the ESM). Barrett-Joyner-Halendra (BJH) analysis was also used to characterize the porosity in each sample (Figs. S12 and S13 in the ESM). MnMoN<sub>2</sub> and Co<sub>0.6</sub>Mo<sub>1.4</sub>N<sub>2</sub> showed some mesoporosity with average pore sizes of 33 and 31 nm, respectively. In comparison, WN had mesopores with an average size of 7 nm. Mo<sub>2</sub>N showed a very large BJH spectrum while the other samples did not show mesoporosity, consistent with the BET isotherms. We explain the observed mesoporosity with the following: The nitridation step releases the

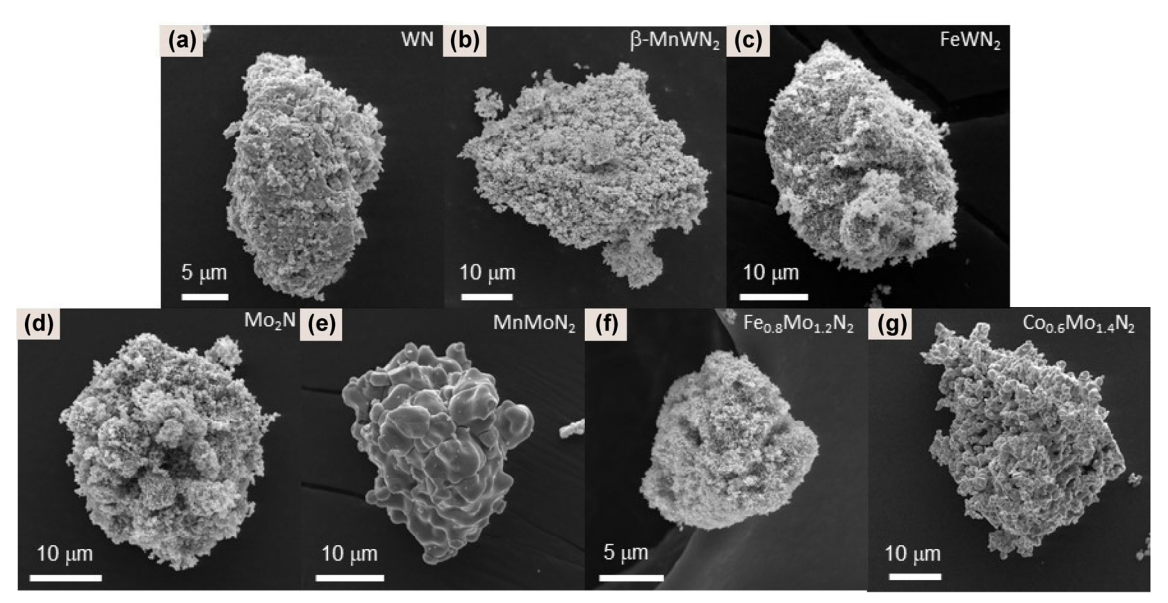


Figure 3 SEM results for (a) WN, (b) β-MnWN<sub>2</sub>, (c) FeWN<sub>2</sub>, (d) Mo<sub>2</sub>N, (e) MnMoN<sub>2</sub>, (f) Fe<sub>0.8</sub>Mo<sub>1.2</sub>N<sub>2</sub>, and (g) Co<sub>0.6</sub>Mo<sub>1.4</sub>N<sub>2</sub>.

oxygen faster than the incorporation of the nitrogen atoms, resulting in void space which coalesces into mesopores. For samples with no mesoporosity, we hypothesize that the length scale of porosity is larger than what can be observed with N2 adsorption. The results of the surface area and porosity analysis are shown in Table S3 in the ESM.

To characterize the electrochemical properties, we prepare a TMN thin-film electrode using a solution-casting approach. Each TMN powder was mixed with an acetylene black carbon support and a Nafion ionomer in a 1:1:1 mass ratio. The TMN, carbon, and Nafion mixture was dispersed in a 1:4 volumetric mixture of isopropanol and water. The final ink composition was: 1 mg<sub>catalyst</sub>·mL<sup>-1</sup>, 1 mg<sub>carbon</sub>·mL<sup>-1</sup>, and 1 mg<sub>Nafion</sub>·mL<sup>-1</sup>. The TMN thin-film electrode was made by solution-casting 15 µL of the catalyst ink on a glassy carbon electrode. The ink was allowed to dry under a controlled atmosphere overnight. The ORR activity was then measured using a rotating disk electrode (RDE) at 1,600 RPM in an O2-saturated 0.1 M HClO4 electrolyte (Figs. 4(a) and 4(b)).

To assess the intrinsic activity difference between the TMNs, we use a specific activity comparison, which normalizes the observed ORR current to the surface area of the catalyst to eliminate the surface area effect, i.e., less intrinsically active catalysts can appear more active than more intrinsically active catalysts if the former has more surface area. We use the BET area as an approximation to the surface area correction. Many groups have discussed the accuracy and the drawbacks of this approach [27]. We point our readers to these works for further details on our chosen approach. When the intrinsic ORR activity is used for comparison, WN shows minimal specific ORR activity (0.05 μA·cm<sub>catalyst</sub><sup>-2</sup> at 0.4 V vs. RHE). The activity improves with 3d metal incorporation. Specifically, β-MnWN<sub>2</sub> has a specific activity of 1.5  $\mu A \cdot cm_{catalyst}^{-2}$  at 0.4 V vs. RHE, while FeWN<sub>2</sub> has a specific activity of 13.3 μA·cm<sub>catalyst</sub><sup>-2</sup> at the same potential (Fig. 4(d)). Mo<sub>2</sub>N is substantially more active than WN, showing moderate ORR specific activity of 3.4 μA·cm<sub>catalyst</sub><sup>-2</sup> at 0.6 V vs. RHE. However, unlike WN, when a 3d transition metal is added to the Mo-based TMNs, the ORR activity can either increase or decrease depending on the 3d chemistry. At 0.6 V vs. RHE, MnMoN<sub>2</sub> (1.4 µA·cm<sub>catalyst</sub><sup>-2</sup>) is less active than Mo<sub>2</sub>N, while Fe<sub>0.8</sub>Mo<sub>1.2</sub>N<sub>2</sub> (5.3 μA·cm<sub>catalyst</sub><sup>-2</sup>) and Co<sub>0.6</sub>Mo<sub>1.4</sub>N<sub>2</sub> (11.6 μA·cm<sub>catalyst</sub><sup>-2</sup>) are more active than Mo<sub>2</sub>N (Fig. 4(c)). We characterize the ORR specific activity stability of our highest performing sample, Co<sub>0.6</sub>Mo<sub>1.4</sub>N<sub>2</sub>, and show that it is stable for at least 14 h when cycled between 0.1 and 0.75 V vs. RHE at 10 mV·s<sup>-1</sup>, consistent with Ref. [17] (Fig. S14 in

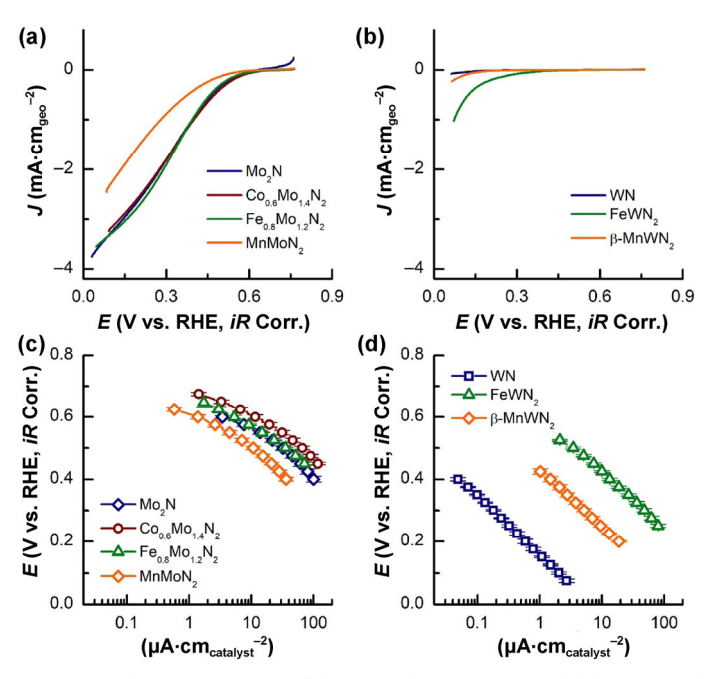


Figure 4 Polarization curves of binary and ternary (a) molybdenum- and (b) tungsten nitride-based catalysts measured using thin-film RDE at 1,600 RPM. Geometric current densities in (a) and (b) were measured in O2-saturated 0.1 M HClO<sub>4</sub> at 10 mV·s<sup>-1</sup>. Tafel plots show the ORR specific activity for (c) molybdenum- and (d) tungsten-based catalysts normalized by the BET surface area. Error bars represent the standard deviation of three independent measurements.

the ESM). Because previous literature results did not report the specific activity of these structures [17, 28, 29], we instead use a mass activity comparison. Our mass activities are within an orderof-magnitude of the previously reported results (Fig. S15 in the ESM). The differences in the ORR activity may come from the differences in the synthesis conditions, which could lead to different particle sizes and surface areas.

We use the ORR activity trend to study the influence of 3d transition metal incorporation on the ORR activity of TMNs. Our observation shows that inclusion of more electronegative 3d transition metals can benefit the ORR in both Mo-based and W-based TMNs (i.e., Co > Fe > Mn). This observation has also been observed in ternary Ti nitride catalysts [30]. Therefore, we hypothesize that 3d transition metal addition affects the ORR activity by electronically interacting with the active Mo-N and W-N moieties. This hypothesis comes from observations in literature that 3d transition metals can be leached out in acid even in the nitride form [14]. Thus, the exposed 3d transition metals on the TMN surface are likely leached out, resulting in an acid-stable shell of Mo-N (or W-N) over the ternary TMNs. The core-shell configuration is similar to Pt-M alloys, where the 3d transition metal (M) is also leached out in acid, leaving behind an acid-stable Pt shell overlayer with a Pt-M core. Our explanation is thus similar to the enhancement mechanism proposed in Pt-M alloys, i.e., we can separate the interaction between the acid-stable Mo-N (or W-N) shell and the ternary TMN core into two categories: the strain and ligand effects. In the former, the interaction comes from the lattice mismatch between the ternary TMN core and the top Mo-N (or W-N) shell, while in the latter, the electronegativity difference of the underlying ternary TMN core can either donate or withdraw electrons away from the top Mo-N/W-N layer. In either scenario, the binding energy of oxygen is affected, causing the ORR activity to change. The impact on the ORR can be either positive or negative, depending on how the oxygen binding energy is precisely affected.

In our Mo-based TMN studies, we see that Co and Fe enhance the activity while Mn decreases the activity. However, when Mn and Fe are incorporated in W-based TMNs, we observe an enhancement in the ORR activity. In both cases, the activity always goes in the order of Mn < Fe (and < Co). Given the importance of the 3d chemistry, we elect to qualitatively explain our result using the ligand effect. For the W-based TMNs, the more electronegative Fe is able to oxidize the W valence state more than Mn, hence the Fe addition results in a more active sample than Mn. In WN, W is least oxidized, making it least active of the studied tungstates. For the Mo-based TMNs, Mo is already relatively oxidized. Mn is not sufficiently electro-negative to reduce the Mo valence state, which causes the ORR activity to drop. Co and Fe, on the other hand, are more electro-negative and thus can oxidize Mo, allowing the compounds to be more active for the ORR. In the hypothesis, both Mo-based and W-based TMNs are more active when Mo or W has higher oxidation states, thereby suggesting that future addition of anion vacancies may further provide a route to increase activity.

Previous X-ray photoelectron spectroscopy (XPS) results for  $Co_{0.6}Mo_{1.4}N_2$  show the presence of  $Mo^{>3+}$  peaks, supporting our hypothesis of charge transfer from  $Co^{3+}$  to  $Mo^{3+}$  [26, 31]. Tracing the oxidation state alone as an assessment of the charge transfer is not straightforward, however, because local structure changes can modify the exact position of the Mo peaks, affecting the oxidation state interpretation. We also note that we cannot eliminate the possibility that the 3d metal addition may affect the terminations in different samples. We make an assumption that this factor does not significantly affect the overall trend. To support this assumption, single crystal studies would be necessary.

Based on this analysis, we can conclude that the general strategy of finding TMNs for ORR catalysis in acid environments is picking an acid-stable TMN and then finding a dopant that can strongly oxidize it. This can be achieved by doping with metals with more d-electrons or introducing anionic vacancies to tune the oxygen binding strength. To further enhance activity, dopant metals which can contribute greater electron density than Co, such as Ni, Cu, or even Zn, should be investigated in the future.

# Acknowledgements

We thank Professor Francis J. DiSalvo (Cornell) for valuable discussions and use of his laboratory facility. The work is supported by the National Science Foundation (NSF) under Grant No. CHE-1805400. This work used the Cornell Center for Materials Research

Shared Facilities which were supported through the NSF Materials Research Science and Engineering Center program (DMR-1120296).

**Electronic Supplementary Material**: Supplementary material (experimental details, additional X-ray diffraction, BET isotherms, BJH pore sizes, and ORR mass activity Tafel plots) is available in the online version of this article at https://doi.org/10.1007/s12274-019-2440-6.

## References

- [1] Gasteiger, H. A.; Kocha, S. S.; Sompalli, B.; Wagner, F. T. Activity benchmarks and requirements for Pt, Pt-alloy, and non-Pt oxygen reduction catalysts for PEMFCs. *Appl. Catal. B: Environ.* **2005**, *56*, 9–35.
- [2] Stamenkovic, V. R.; Fowler, B.; Mun, B. S.; Wang, G.; Ross, P. N.; Lucas, C. A.; Marković, N. M. Improved oxygen reduction activity on Pt<sub>3</sub>Ni(111) via increased surface site availability. *Science* 2007, 315, 493–497.
- [3] Stephens, I. E. L.; Bondarenko, A. S.; Grønbjerg, U.; Rossmeisl, J.; Chorkendorff, I. Understanding the electrocatalysis of oxygen reduction on platinum and its alloys. *Energy Environ. Sci.* 2012, 5, 6744–6762.
- [4] Mani, P.; Srivastava, R.; Strasser, P. Dealloyed binary PtM<sub>3</sub> (M = Cu, Co, Ni) and ternary PtNi<sub>3</sub>M (M = Cu, Co, Fe, Cr) electrocatalysts for the oxygen reduction reaction: Performance in polymer electrolyte membrane fuel cells. *J. Power Sources* 2011, 196, 666–673.
- [5] Lefèvre, M.; Proietti, E.; Jaouen, F.; Dodelet, J. P. Iron-based catalysts with improved oxygen reduction activity in polymer electrolyte fuel cells. *Science* 2009, 324, 71–74.
- [6] Wu, G.; More, K. L.; Johnston, C. M.; Zelenay, P. High-performance electrocatalysts for oxygen reduction derived from polyaniline, iron, and cobalt. *Science* 2011, 332, 443–447.
- [7] Proietti, E.; Jaouen, F.; Lefèvre, M.; Larouche, N.; Tian, J.; Herranz, J.; Dodelet, J. P. Iron-based cathode catalyst with enhanced power density in polymer electrolyte membrane fuel cells. *Nat. Commun.* 2011, 2, 416.
- [8] Zhang, H.; Hwang, S.; Wang, M.; Feng, Z.; Karakalos, S.; Luo, L.; Qiao, Z.; Xie, X.; Wang, C.; Su, D. et al. Single atomic iron catalysts for oxygen reduction in acidic media: particle size control and thermal activation. *J. Am. Chem. Soc.* 2017, 139, 14143–14149.
- [9] Sahraie, N. R.; Kramm, U. I.; Steinberg, J.; Zhang, Y.; Thomas, A.; Reier, T.; Paraknowitsch, J. P.; Strasser, P. Quantifying the density and utilization of active sites in non-precious metal oxygen electroreduction catalysts. *Nat. Commun.* 2015, 6, 8618.
- [10] An, L.; Huang, W.; Zhang, N.; Chen, X.; Xia, D. A novel CoN electrocatalyst with high activity and stability toward oxygen reduction reaction. *J. Mater. Chem. A* 2014, 2, 62–65.
- [11] Abroshan, H.; Bothra, P.; Back, S.; Kulkarni, A.; Nørskov, J. K.; Siahrostami, S. Ultrathin cobalt oxide overlayer promotes catalytic activity of cobalt nitride for the oxygen reduction reaction. J. Phys. Chem. C 2018, 122, 4783–4791.
- [12] Miura, A.; Rosero-Navarro, C.; Masubuchi, Y.; Higuchi, M.; Kikkawa, S.; Tadanaga, K. Nitrogen-rich manganese oxynitrides with enhanced catalytic activity in the oxygen reduction reaction. *Angew. Chem., Int. Ed.* 2016, 55, 7963–7967.
- [13] Wang, L.; Yin, J.; Zhao, L.; Tian, C.; Yu, P.; Wang, J.; Fu, H. Ion-exchanged route synthesis of Fe<sub>2</sub>N-N-doped graphitic nanocarbons composite as advanced oxygen reduction electrocatalyst. *Chem. Commun.* 2013, 49, 3022–3024.
- [14] Sun, T.; Wu, Q.; Che, R.; Bu, Y.; Jiang, Y.; Li, Y.; Yang, L.; Wang, X.; Hu, Z. Alloyed Co–Mo nitride as high-performance electrocatalyst for oxygen reduction in acidic medium. ACS Catal. 2015, 5, 1857–1862.
- [15] Chen, Z.; Higgins, D.; Yu, A.; Zhang, L.; Zhang, J. A review on non-precious metal electrocatalysts for PEM fuel cells. *Energy Environ. Sci.* 2011, 4, 3167–3192.
- [16] Cao, B.; Veith, G. M.; Diaz, R. E.; Liu, J.; Stach, E. A.; Adzic, R. R.; Khalifah, P. G. Cobalt molybdenum oxynitrides: Synthesis, structural characterization, and catalytic activity for the oxygen reduction reaction. *Angew. Chem., Int. Ed.* 2013, 52, 10753–10757.
- [17] Cao, B.; Neuefeind, J. C.; Adzic, R. R.; Khalifah, P. G. Molybdenum nitrides as oxygen reduction reaction catalysts: structural and electrochemical studies. *Inorg. Chem.* 2015, 54, 2128–2136.

- [18] Miura, A.; Wen, X.; Abe, H.; Yau, G.; DiSalvo, F. J. Non-stoichiometric Fe<sub>x</sub>WN<sub>2</sub>: Leaching of Fe from layer-structured FeWN<sub>2</sub>. *J. Solid State Chem.* 2010, 183, 327–331.
- [19] Luo, J.; Tian, X.; Zeng, J.; Li, Y.; Song, H.; Liao, S. Limitations and improvement strategies for early-transition-metal nitrides as competitive catalysts toward the oxygen reduction reaction. ACS Catal. 2016, 6, 6165–6174.
- [20] Grins, J.; Käll, P. O.; Svensson, G. Synthesis and structural characterisation of MnWN<sub>2</sub> prepared by ammonolysis of MnWO<sub>4</sub>. J. Mater. Chem. 1995, 5, 571–575.
- [21] DiSalvo, F. J.; Clarke, S. J. Ternary nitrides: A rapidly growing class of new materials. Curr. Opin. Solid State Mater. Sci. 1996, 1, 241–249.
- [22] Bern, D. S.; Olsen, H. P.; zur Loye, H. C. Synthesis, electronic and magnetic characterization of the ternary nitride (Fe<sub>0.8</sub>Mo<sub>0.2</sub>)MoN<sub>2</sub>. *Chem. Mater.* 1995, 7, 1824–1828.
- [23] Bem, D. S.; Lampe-Önnerud, C. M.; Olsen, H. P.; zur Loye, H. C. Synthesis and structure of two new ternary nitrides: FeWN<sub>2</sub> and MnMoN<sub>2</sub>. *Inorg. Chem.* 1996, 35, 581–585.
- [24] Panda, R. N.; Gajbhiye, N. S. Chemical synthesis and magnetic properties of nanocrystalline FeMoN<sub>2</sub>. J. Cryst. Growth 1998, 191, 92–96.
- [25] Jackson, S. K.; Layland, R. C.; zur Loye, H. C. The simultaneous powder

- X-ray and neutron diffraction refinement of two η-carbide type nitrides, Fe<sub>3</sub>Mo<sub>3</sub>N and Co<sub>3</sub>Mo<sub>3</sub>N, prepared by ammonolysis and by plasma nitridation of oxide precursors. *J. Alloys Compd.* **1999**, *291*, 94–101.
- [26] Cao, B.; Veith, G. M.; Neuefeind, J. C.; Adzic, R. R.; Khalifah, P. G. Mixed close-packed cobalt molybdenum nitrides as non-noble metal electrocatalysts for the hydrogen evolution reaction. *J. Am. Chem. Soc.* 2013, 135, 19186– 19192
- [27] Jung, S.; McCrory, C. C. L.; Ferrer, I. M.; Peters, J. C.; Jaramillo, T. F. Benchmarking nanoparticulate metal oxide electrocatalysts for the alkaline water oxidation reaction. *J. Mater. Chem. A* 2016, 4, 3068–3076.
- [28] Cao, B. Investigations of non-noble metal based oxynitrides and nitrides as electrocatalysts for oxygen reduction reaction and hydrogen evolution reaction. Ph.D. Dissertation, Stony Brook University, New York, 2014.
- [29] Zhong, H.; Zhang, H.; Liang, Y.; Zhang, J.; Wang, M.; Wang, X. A novel non-noble electrocatalyst for oxygen reduction in proton exchange membrane fuel cells. J. Power Sources 2007, 164, 572–577.
- [30] Tian, X.; Luo, J.; Nan, H.; Fu, Z.; Zeng, J.; Liao, S. Binary transition metal nitrides with enhanced activity and durability for the oxygen reduction reaction. J. Mater. Chem. A 2015, 3, 16801–16809.
- [31] Hada, K.; Nagai, M.; Omi, S. Characterization and HDS activity of cobalt molybdenum nitrides. J. Phys. Chem. B 2001, 105, 4084–4093.



# Erratum to: Influence of 3d transition-metal substitution on the oxygen reduction reaction electrocatalysis of ternary nitrides in acid

Kevin E. Fritz<sup>1</sup>, Yichen Yan<sup>1</sup>, and Jin Suntivich<sup>1,2</sup> ( )

# Erratum to

Nano Research 2019, 12(9): 2307–2312 https://doi.org/10.1007/s12274-019-2440-6

The NSF number in Acknowledgements in page 2311 was unfortunately wrong,

#### instead of

The work is supported by the National Science Foundation (NSF) under Grant No. CHE-1805400.

#### It should read

The work is supported by the National Science Foundation (NSF) under Grant No. CHE-1665305.

The online version of the original article can be found at https://doi.org/10.1007/s12274-019-2440-6

<sup>&</sup>lt;sup>1</sup> Department of Materials Science and Engineering, Cornell University, Ithaca, New York 14850, USA

<sup>&</sup>lt;sup>2</sup> Kavli Institute at Cornell for Nanoscale Science, Ithaca, New York 14850, USA

<sup>©</sup> Tsinghua University Press and Springer-Verlag GmbH Germany, part of Springer Nature 2020